http://dx.doi.org/10.5935/0103-5053.20150164

J. Braz. Chem. Soc., Vol. 26, No. 9, 1871-1878, 2015.
Printed in Brazil - ©2015 Sociedade Brasileira de Química
0103 - 5053 $6.00+0.00

Article

Bifunctional Porous SiO_2 Complex Nanoparticles with Properties of Enzymatic Catalysis and Optical Oxygen Sensing

Jun Huang,* Kun Li, Huichao Liu and Liyun Ding

National Engineering Laboratory for Fiber Optic Sensing Technology and Key Laboratory of Fiber Optic Sensing and Information Processing, Wuhan University of Technology, 430070 Wuhan, China

The porous fluorescent SiO_2 nanoparticles encapsulating photosensitizer $Ru(bpy)_3Cl_2$ were prepared by Stöber method and used as a carrier to immobilize glucose oxidase (GOD) to form the bifunctional porous SiO_2 complex nanoparticles (BPSCNp) with the properties of enzymatic catalysis and optical oxygen sensing. The optimal immobilization conditions are as follows: hexadecyltrimethyl ammonium bromide (APTES) concentration of 2% (v/v), glutaraldehyde (GA) concentration of 1.0% (v/v), and pH of 6.5, GOD amount of 4.0 mg in 40 mg of carrier. BPSCNp showed maximal catalytic activity at pH 6.0 and 50 °C. After immobilization, the thermal storage and operation stability of GOD were improved remarkably. After kept at 4 °C for 30 days, BPSCNp and free GOD retained 68% and 35% of initial activity, respectively. BPSCNp maintained 58% of its initial activity after 7 consecutive operations and 30% after 15 consecutive operations. The fluorescence of BPSCNp could be quenched effectively by oxygen. There was a good linear relationship between $\tan\phi_0/\tan\phi$ and O_2 concentration in the range of 0 to ca. 90%. BPSCNp had a highly reproducible response to oxygen with the response time of 20 s. BPSCNp might be used as the sensing material and have potential application in multi parameter fiber optic biosensor based on enzyme catalysis and oxygen consumption.

Keywords: BPSCNp, bifunctional properties, enzymatic catalysis, stability, oxygen sensing

Introduction

Silica nanoparticles have been used in a variety of biological applications due to their resistance to microbial attack, stability in aqueous solutions, low toxicity, ability to be functionalized, and penetrability through biomembranes.[1,2] Luminescent silica nanoparticles offer significant advantages compared to free dyes.[3,4] The encapsulation of luminescent molecules in silica nanoparticles often increases their photostability and emission quantum yield because of their isolation from possible quenchers such as molecular oxygen and water.[5,6] Bright and stable luminescent labels are often required for many applications, such as drug delivery,[7,8] bioimaging,[9] cell tracking,[10] and sensing.[11-14]

Fiber optic biosensors have many advantages such as high sensitivity, fast response, immunity from electrical interference, long distance sensing, and low cost compared with electrical sensors and electrochemical sensors.[15] As a branch of fiber optic sensor, the enzyme based fiber optic biosensors have great potential to be applied in many fields. However, these sensors often suffer from the drawback of nature enzymes such as poor stability, complicated preparation and impossibility of reuse. To overcome these problems, the immobilized enzymes offer several advantages including their reuse, possibility of better control of reactions, ease removal from the reaction medium and improving in the stability. SiO_2 nanoparticles are highly compatible with enzymes[16,17] and were used for fabrication of amperometric glucose sensor.[18] Most of the reported sensing materials for fiber optic biosensor based on enzyme catalysis usually consist of two parts,[19-21] the optical sensing part and catalytic enzyme part. If the SiO_2 nanoparticles containing photosensitizer are used to immobilize enzyme to form the biofunctional SiO_2 complex nanoparticles with the properties of enzymatic catalysis and optical oxygen sensing, the catalysis effect of enzyme can arrive at the photosensitizer directly, which will improve the performance of fiber optic biosensor. Furthermore, by preparing different immobilized enzyme

*e-mail: hjun@whut.edu.cn

on luminescent silica nanoparticles and controlling the enzyme performance, it will be possible to develop the multi parameter fiber optic biosensor based on enzyme catalysis and oxygen consumption.

Although the synthesis of $Ru(bpy)_3Cl_2$ entrapped in SiO_2 nanoparticles[22-24] and porous SiO_2 nanoparticles[25] were reported, and the immobilization of glucose oxidase (GOD) on silica was also reported,[26,27] there have been no publications on immobilizing GOD on porous fluorescent SiO_2 nanoparticles to form the bifunctional nanoparticles with the properties of enzymatic catalysis and optical oxygen sensing.

In this work, we prepared the porous SiO_2 nanoparticles encapsulating the photosensitizer $Ru(bpy)_3Cl_2$ and immoblilized GOD on the surface of the luminescent SiO_2 nanoparticles to form bifunctional porous SiO_2 complex nanoparticles (BPSCNp). Immobilization conditions including pH, initial concentration of hexadecyltrimethyl ammonium bromide (APTES), glutaraldehyde (GA) and GOD were investigated and optimized. The properties of BPSCNp including catalytic activity as a function of pH and temperature, thermal, storage and operational stability were studied. The oxygen sensing properties of BPSCNp were also studied. Our results show that BPSCNp have both the improved catalytic performance and excellent oxygen sensing properties, showing a promising application potential in multi parameter fiber optic biosensor based on enzyme catalysis and oxygen consumption.

Experimental

Materials

GOD (E.C. 1.1.3.4, 100 U mg^{-1}) was obtained from Aspergillusniger. Glucose, $Ru(bpy)_3Cl_2$ (99.0%), hexadecyltrimethyl ammonium bromide (CTAB, 99.0%) were purchased from Sigma-Aldrich. APTES (97.0%) was purchased from Alfa Aesar. Tetraethoxysilane (TEOS, 99.9%) and GA (25% in aqueous solution) were purchased from Sinopharm Chemical Reagent Co. All reagents were purchased with analytical grade and used without further purification. Double-distilled water was used throughout the experiments.

Preparation of porous fluorescent SiO_2 nanoparticles

The porous fluorescent SiO_2 nanoparticles were prepared according to Rossi *et al.*,[28] but with modification. Briefly, 15 mL of ethanol (95%, v/v) was mixed with 7.0 mL of ammonium hydroxide (28-30 wt.%) and 0.05 g of CTAB to form solution 1. 3.7 mL of ethanol (95%, v/v) was mixed with 1.3 mL of TEOS and 3.0 mL of $Ru(bpy)_3Cl_2$ (0.5 mg mL^{-1}) to form solution 2. Under stirring, solution 1 was slowly poured into solution 2. Then, the mixed solution was stirred for 2 h at 25 °C (room temperature). The precipitate was collected by centrifugation (10000 rpm, 10 min) and washed with water and ethanol four times. Finally the pore-generating template, CTAB, was removed by refluxing in acid ethanol solution (70 °C, 24 h). The obtained porous fluorescent SiO_2 nanoparticles were sufficiently dried at 80 °C in vacuum.

Preparation of BPSCNp

4.0 mL of prepared APTES solution (2%, v/v) was stirred for 40 min aimed to sufficient hydrolyzation, followed by the addition of 40 mg of porous fluorescent SiO_2 nanoparticles. The mixture solution was stirred for 18 h at 25 °C. The modified nanoparticles were centrifuged with water and dispersed in 4 mL of phosphate buffer (PBS, 0.01 mol L^{-1}, pH 7.0). After 160 μL of GA (25%, v/v) was added, and the resulting mixture was stirred for 1 h. The precipitate was centrifuged 4 times with water. After collection, the activated porous fluorescent SiO_2 nanoparticles were obtained. In a tube, 4.0 mg of GOD was dissolved in 6 mL of PBS buffer (0.2 mol L^{-1}, pH 6.5) and the activated porous fluorescent SiO_2 nanoparticles were added in it. The reaction was kept for 24 h with regular shaking at 4 °C. To remove free GOD, the nanoparticles were centrifuged with PBS buffer thoroughly. BPSCNp were finally collected, and stored in PBS buffer (0.2 mol L^{-1}, pH 6.0) at 4 °C. Following the Bradford method,[29] by substracting the residual free GOD content in the solution from the initial free GOD content the amount of GOD protein loaded onto the porous fluorescent SiO_2 nanoparticles was measured.

Assay of GOD activity

The activity of GOD was monitored using a colorimetric method.[30] GOD catalyzed the oxidation of β-D-glucose to gluconic acid, while H_2O_2 was generated concurrently. Because of the presence of peroxidase, the generated H_2O_2 reacted with phenol and 4-aminoantipyrine, and formed the red quinoneimine dye complex. The GOD activity was measured, in triplicate, by recording the absorbance of the red dye at 510 nm at which the dye complex exhibited its maximal adsorption. At 25 °C and pH 7.0, the amount of GOD which oxidized 1 μmol of substrate *per* min was defined as one unit of GOD activity.

Stability of GOD

To investigate the thermal stability of BPSCNp, the enzyme activity was measured in different time of incubation at 60 °C. The storage stability of BPSCNp was determined by storing it at 4 °C for 30 days and measuring its residual activity every five days. As a control experiment, enzyme activity of free GOD was determined in the same condition.

To study the operation stability of BPSCNp, several consecutive operation cycles were carried out by oxidizing the glucose. After finishing each oxidation cycle, PBS buffer (0.1 mol L^{-1}, pH 7.0) was used to wash BPSCNp for several times and the procedure was performed repeatedly with a fresh aliquot of the substrate.

Optical oxygen sensing property of BPSCNp

The detecting system of oxygen sensing property consists of a lock-in amplifier, a light emitting diode (LED) which has excitation wavelength of 416 nm as the light source, a detecting head and a computer for data processing (Figure 1a). 50 mg of BPSCNp were simply fitted in the concave part of the detection head (Figure1b) and allowed them to contact with air.

The detection was based on the fluorescence quenching (Figure 1c). The oxygen concentration was detected by detecting the fluorescence of $Ru(bpy)_3Cl_2$ quenched by oxygen. Since a lock-in amplifier is used, the quechening could be described by the equation (1):

$$\frac{\tan\phi_0}{\tan\phi} = 1 + K_{sv}[Q] \quad (1)$$

where ϕ_0 and ϕ are the phase delays of the detecting head in the absence and in the presence of the oxygen, respectively, and K_{sv} is the Stern-Volmer constant. [Q] is the oxygen concentration. By detecting the data of phase delay ϕ the quantification of oxygen concentraton is achieved.

Characterizations

The morphologies of the porous SiO_2 nanoparticles were observed using a field emission scanning electron microscope (FESEM) (JSM-5610LV, JEOL) operated at 10 kV. Before FESEM test, the samples were evenly dispersed in aqueous solution through ultrasonic, then they were dropped on the conductive adhesive and dried at room temperature. Infrared (IR) spectrum was recorded on a Thermo Nicolet Nexus Fourier transform (FTIR) spectrometer with the standard KBr pellet method. Pore size and porosity measurements were performed by the Brunauer-Emmett-Teller (BET) method on a ASAP 2020 instrument. Particle size was determined by particle size analyzer (Mastersizer-2000). By substracting the residual $Ru(bpy)_3Cl_2$ in the upper centrifugal liquid from the initial dye amount, the $Ru(bpy)_3Cl_2$ content in the porous fluorescent SiO_2 nanoparticles was measured. Fluorescent quantum yields were detected by a fluorospectrophotometer (Hitachi F-4500), using Rhodamine B as standard substance. The activities of BPSCNp were measured by spectrophotometer (UV-2450, Shimadzu). A loch-in amplifier (SR830, Standford Research System) was used for measuring the phase delay of BPSCNp.

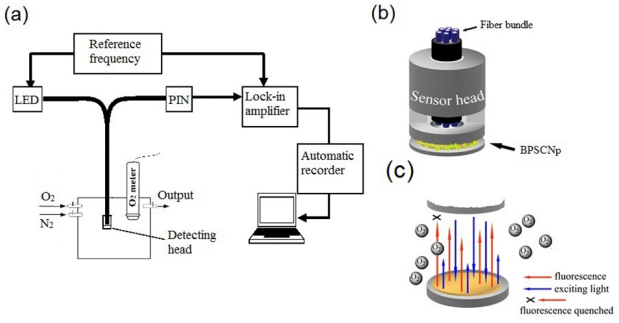

Figure 1. Detecting system for oxygen sensing property in (a) and the model of detection head containing BPSCNp in (b); and the process of BPSCNp fluorescence quenched by oxygen in (c).

Results and Discussion

The Stöber synthesis method was used to prepare highly luminescent monodispersed SiO_2 nanoparticles that encapsulate indicator $Ru(bpy)_3Cl_2$. The formation of SiO_2 nanoparticles consisted of hydrolysis, nucleation and particle growth, and hydrolysis is the controlling process. Meanwhile, CTAB was playing a role as the pore-formed template. The particles were kept in a water solution for 1 month. Low fluorescent degradation indicated that the particles were photostable with minimal indicator leakage. Scanning electron microscopy (SEM) images of the porous fluorescent SiO_2 nanoparticles are shown in Figure 2a. It can be seen that the SiO_2 nanoparticles embedding $Ru(bpy)_3Cl_2$ are porous monodispersed spheres. After GOD was immobilized on the porous fluorescent SiO_2 nanoparticles to form BPSCNp, its surface was smooth because GOD was loaded on it (Figure 2b).

For the porous fluorescent SiO_2 nanoparticles, the BET surface area and average pore width were measured to be 276.0 m^2 g^{-1} and 5.67 nm, respectively. However, after the GOD immobilization, the BET surface area of the SiO_2 nanoparticles was measured to be117.4 m^2 g^{-1} while the average pore width was measured to be 5.58 nm (Table 1).

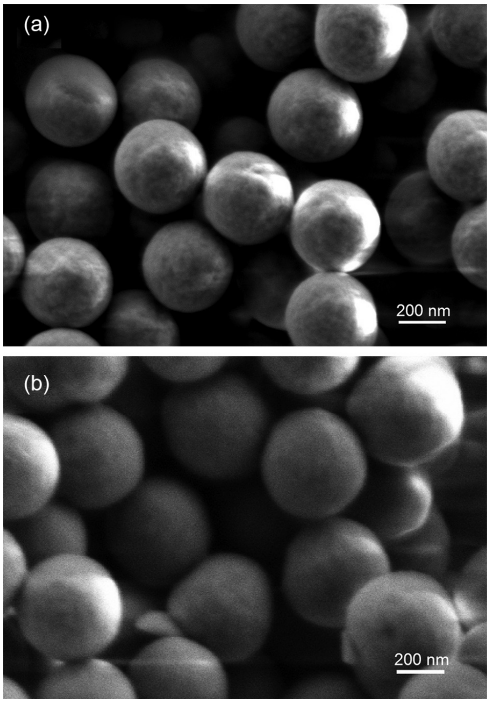

Figure 2. SEM of porous fluorescent SiO_2 nanoparticles in (a) and BPSCNp in (b).

The GOD immobilization significantly reduced the BET surface area of the nanoparticles, but had less influence on their average pore width.

The mean particle size of porous fluorescent SiO_2 nanoparticles and BPSCNp were detected (Table 1). It can be seen that the size of BPSCNp increased 24 nm after the immobilization of GOD on porous fluorescent SiO_2 nanoparticles. The $Ru(bpy)_3Cl_2$ content in the porous fluorescent SiO_2 nanoparticles was measured to be 0.072% (m/m). Since the amount of GOD protein loaded onto the porous fluorescent SiO_2 nanoparticles can be detected, the $Ru(bpy)_3Cl_2$ content in BPSCNp could be determined to be 0.066% (m/m) (Table 1).

The fluorescent quantum yields for porous fluorescent SiO_2 nanoparticles and BPSCNp were detected using Rhodamine B as standard substance (Table 1). The fluorescent quantum yield of BPSCNp is lower than that of porous fluorescent SiO_2 nanoparticles. The reason is probably that the immobilization of GOD could slightly quench the fluorescence of dye and reduce the fluorescent quantum yields.

Figure 3 shows the FTIR spectrum of porous fluorescent SiO_2 complex nanoparticles. The characteristic absorption of $Ru(bpy)_3Cl_2$ was observed at 1629 cm^{-1}. The band at 1096 cm^{-1} corresponds to Si-O-Si antisymmetric stretching vibrations, and the band at 799 cm^{-1} corresponds to Si-O-Si bending vibration, indicating the existence of SiO_2 in the complex nanoparticles. Obviously, $Ru(bpy)_3Cl_2$ is doped in the porous silica nanoparticles.

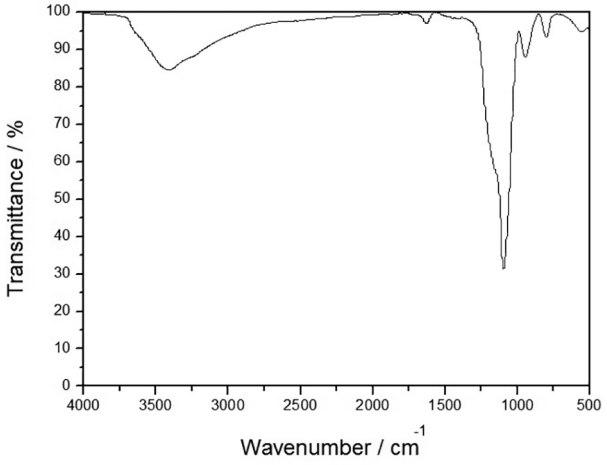

Figure 3. FTIR spectrum of porous fluorescent SiO_2 complex nanoparticles.

The effect of APTES concentration on the activity of BPSCNp is shown in Figure 4a. As a coupling agent, APTES can chemically react with both silica surface and aldehyde units on GA.

The activity of immobilized GOD increases when APTES concentration increases from 1% (v/v) to 2% (v/v) and reaches the maximum when the APTES concentration is 2% (v/v). Further increase of APTES concentration causes a sharp decline in the activity. It was known that the three methoxy groups on each APTS molecule allow many APTS molecules to connect into complex network structures.[31,32] When the APTES concentration is higher, the formation of complex network from APTES molecules

Table 1. Properties of porous fluorescent SiO_2 nanoparticles and BPSCNp

Property	Porous fluorescent SiO_2 nanoparticles	BPSCNp
BET surface area / $m^2\ g^{-1}$	276.0	117.4
Average pore width / nm	5.67	5.58
Mean particle size / nm	342	366
$Ru(bpy)_3Cl_2$ content / (%, m/m)	0.072 ± 0.004	0.066 ± 0.003
Quantum yield: λ_{max} / 600 nm	0.0873 ± 0.0052	0.0704 ± 0.0042

can join SiO_2 nanoparticles together, which will cause irreversible coagulation[33] and lower activity.

GA is a bifunctional crosslinking agent. One aldehyde on GA molecule connects with the free amino on the surface of aminated porous fluorescent SiO_2 nanoparticles to form the imine linkage (–NH=CH) and the other aldehyde on GA molecule reacts with the free amino in GOD. The effect of GA concentration on the activity of immobilized GOD is shown in Figure 4b. The activity of immobilized GOD increases with the increase of GA concentration from 0.5% (v/v) to 1.0% (v/v) and reaches a maximum value at 1.0% (v/v). The activity decreases rapidly when the GA concentration is higher than 1.0% (v/v). The reason is probably that GA is also a protein denaturing agent and higher GA concentration can lead to GA cross-linking with each other, which could cause the decrease of enzyme activity.

The pH effect on the immobilization of GOD is shown in Figure 4c. With the increase of pH from 5.0 to 6.5, the relative activity of immobilized GOD increases and reaches its maximal value at pH 6.5. When pH increases further, the relative activity of immobilized GOD decreases. The best pH for GOD immobilization is 6.5. At acidic pH, GOD is negatively charged,[34] and the aminated SiO_2 nanoparticles is positively charged. When the medium is acidic, free GOD molecules absorb on the surface of aminated SiO_2 nanoparticles by electrostatic interaction, and amino groups of GOD are easily cross-linked by the aldehyde groups of activated SiO_2 nanoparticles via the Schiff-base route. However, if the medium is more acidic the formation of Schiff-base in the cross-linking process can be hindered, which will have negative effect on the GOD immobilization.

As shown in Figure 4d, the best supply amount of GOD is 4.0 mg in 40 mg of SiO_2 nanoparticles under the optimal immobilization condition and higher GOD amount declines the activity of immobilized enzyme. The increase of GOD content is benefit to enzyme immobilization until the saturation of enzyme occurs, further increase of GOD content will probably lead to special steric hindrance which declines the enzyme activity.

After the immobilization at optimal conditions, the amount of immobilized GOD was determined to be

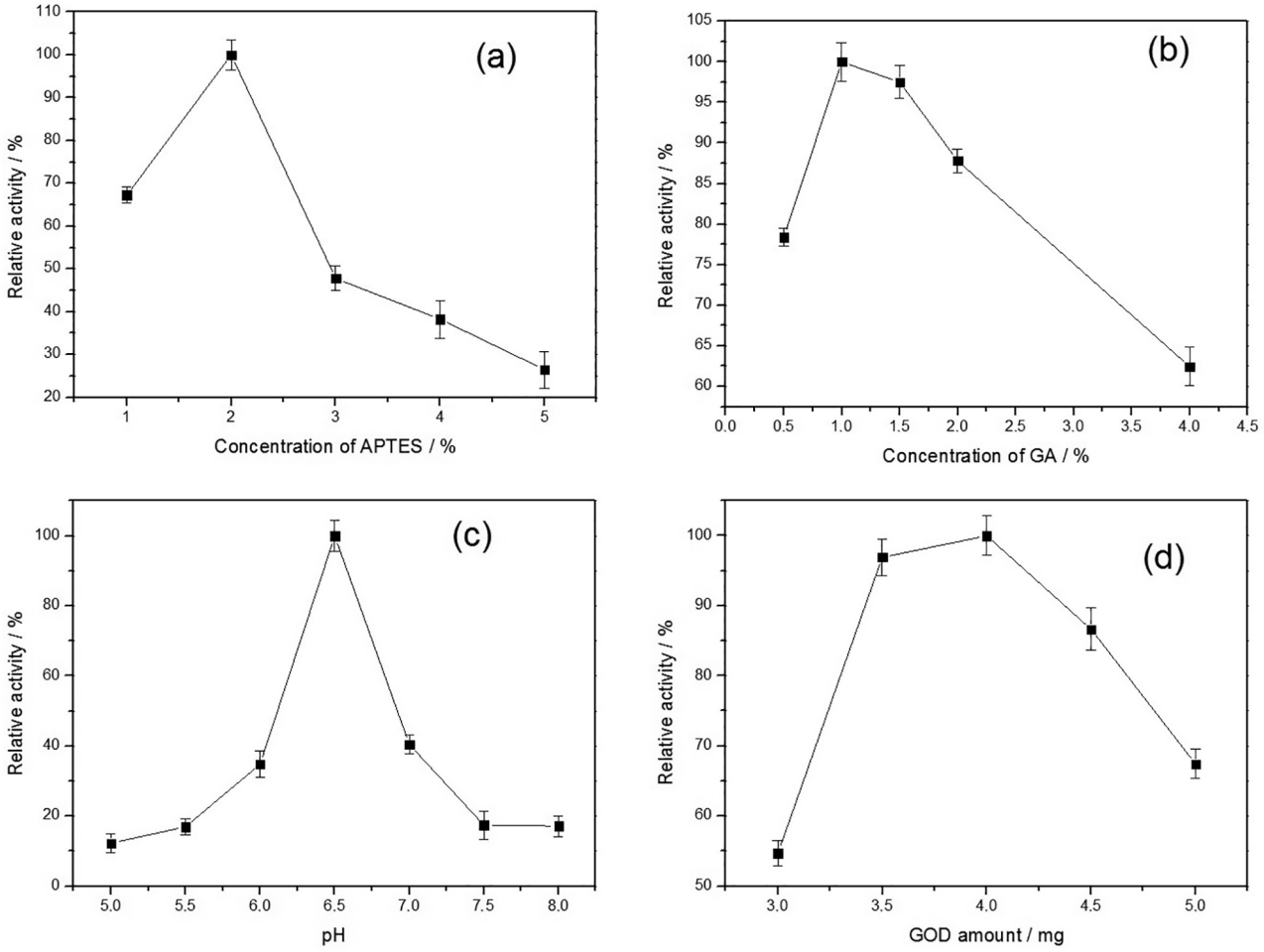

Figure 4. Effect of APTES concentration in (a), GA concentration in (b), solution pH in (c) and GOD amount in (d) on the immobilization of GOD on porous fluorescent SiO_2 nanoparticles.

82.6 mg g^{-1}, suggesting that BPSCNp is a good carrier for GOD immobilization.

The pH has significant effect on enzyme activity. As shown in Figure 5a, in the range from pH 5.0 to 7.5, the activities of GOD of BPSCNp and free GOD increase from pH 5.0 to pH 6.0 and reach their maximal values at pH 6.0. After pH 6.0, with the increase of pH, the activities of BPSCNp decreases slightly while the activity of free GOD decreases sharply. Compared with the free GOD, BPSCNp have a broader workable pH range, indicating that GOD increases the resistance ability to acid and alkali via immobilization.

The effect of temperature on the activity of free GOD and BPSCNp was studied in the temperature range of 20 °C to 80 °C. The results are shown in Figure 5b. The activity of free GOD is strongly dependent on temperature, with the optimal temperature being observed at 30 °C. The BPSCNp exhibits the optimal activity at 50 °C and shows a higher activity (more than 60% of its initial activity) at the temperature from 20 °C to 60 °C, indicating that BPSCNp can be used effectively in a broader temperature range.

As shown in Figure 5c, with the incubation time increases at 60 °C, a sharp decline appears in the activity of free enzyme, but the activity of BPSCNp decreases much slowly. After 60 min of incubation, the activity of free enzyme drops to about 25% of its initial activity, while BPSCNp remains 70% of its initial activity. It indicates that the immobilization of enzyme on the porous fluorescent SiO_2 nanoparticles can inhibit the conformational changes, which makes the structure of enzyme molecules more stable at a high temperature and leads to an improviment on the thermal stability.

The storage stabilities of free enzyme and BPSCNp were studied, as shown in Figure 5d. After kept at 4 °C for 30 days, BPSCNp retained 68% of its initial activity while the activity of free GOD was reduced to 35% of its initial activity. It indicates that the storage stability of GOD was improved after the immobilization on fluorescent SiO_2 nanoparticles.

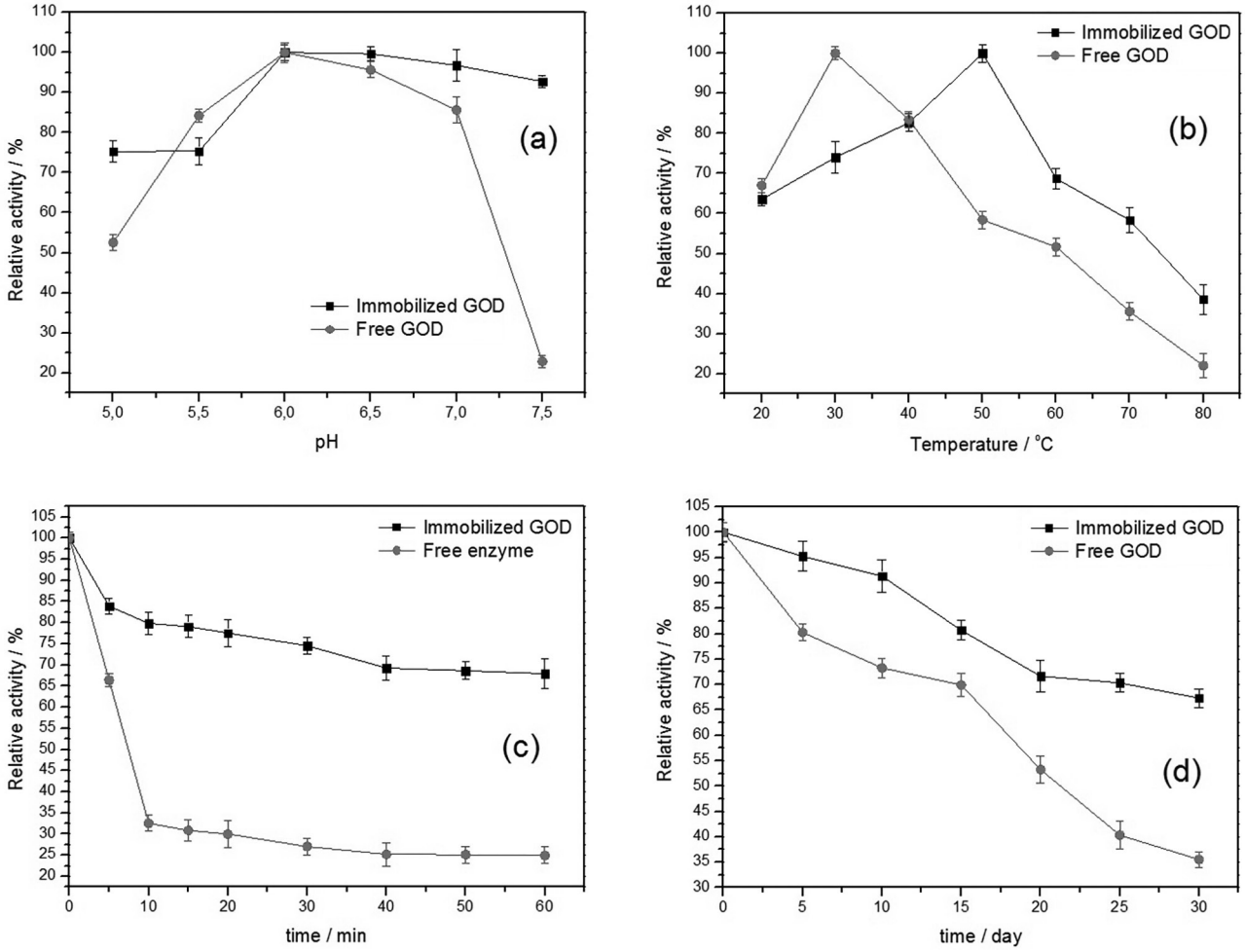

Figure 5. Effect of pH on the catalytic activity of free GOD (●) and BPSCNp (■) in (a); effect of temperature on the catalytic activity of free GOD (●) and BPSCNp (■) in (b); thermal stability of free GOD (●) and BPSCNp (■)in (c); storage stability of free GOD (●) and BPSCNp (■) in (d).

The operation stability of BPSCNp was also studied, as shown in Figure 6. BPSCNp retains 58% of its initial activity after 7 consecutive operations and 30% after 15 consecutive operations, revealing a good operation stability. Probably, the loss of BPSCNp should be a reason for the gradual reduction of activity because it is difficult to collect total immobilized GOD after the cycling experiments.

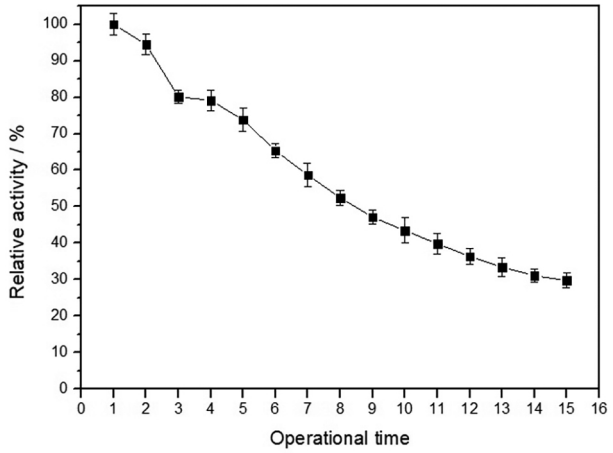

Figure 6. Operational stability of BPSCNp.

The fluorescence of BPSCNp could be quenching effectively by molecular oxygen. With the increase of oxygen concentration, the relative phase delay of BPSCNp,ϕ, increases, as shown in Figure 7. It can be seen that there is a good linear relationship between $\tan\phi_0 / \tan\phi$ and O_2 concentration in the range of 0 to ca. 90%, which was defined by the equation of $y = 0.0005916x + 1.00$ and $R^2=0.9617$, ϕ was the difference between the phase delay of BPSCNp with certain O_2 concentration and with no O_2 (100%, N_2). The detection limit of the detecting system is 0.01%(v/v).

The fluorescence dynamic responses of BPSCNp to pure N_2 and O_2 are shown in Figure 8. It shows that the relative phase delay changes quickly when BPSCNp were exposed to the cycles of pure N_2, pure O_2 , respectively. It had a highly reproducible and reversible response to O_2, showing a good repeatability. The response time could be 20 s, which is rather fast for an oxygen sensing material.

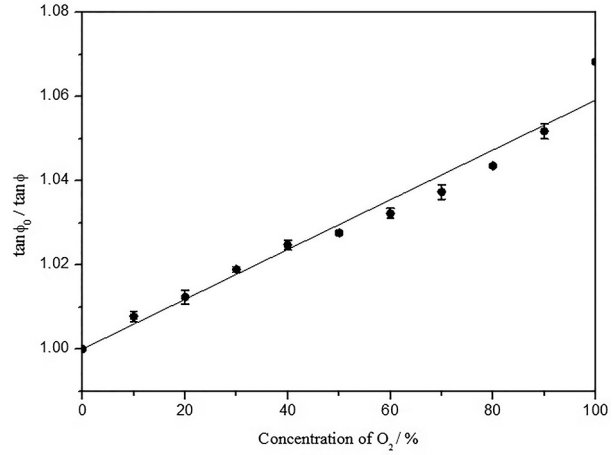

Figure 7. Relationship between $\tan\phi_0 / \tan\phi$ and O_2 concentration.

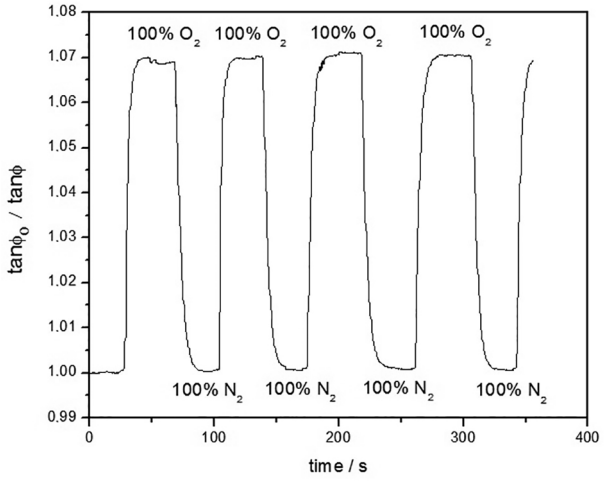

Figure 8. Fluorescence dynamic responses of BPSCNp to pure N_2 and O_2.

When the temperature changed in the range of 10°C to ca. 40°C, there is no obvious difference in the detection results. However, if the temperature is higher than 40°C, the difference in the detection results could not be ignored and the temperature compensation should be performed.[35]

Conclusion

Porous SiO_2 nanoparticles encapsulating photosensitizer $Ru(bpy)_3Cl_2$ were prepared by a modified Stöber method. GOD was immobilized on the porous fluorescent SiO_2 nanoparticles to form BPSCNp and the optimized immobilization conditions were achieved. The optimal catalytic pH and temperature were achieved to be 6.0 and 50 °C, respectively. Compared with free GOD, BPSCNp perform more effectively in a broad temperature range of 20 to ca. 60 °C. Moreover, the thermal storage and operational stability of GOD are improved after immobilization, indicating the porous fluorescent SiO_2 nanoparticles is a favorable carrier for enzyme immobilization. BPSCNp have excellent oxygen sensing property. BPSCNp with properties of enzymatic catalysis and optical oxygen sensing will probably have great application potential in multi parameter fiber optic biosensor based on enzyme catalysis and oxygen consumption.

Acknowledgements

This study was financially supported by National Natural Science Foundation of China (No: 61377092).

References

1. Silveira, G. Q.; Ronconi, C. M.; Vargas, M. D.; Gilb, R. A. S. S.; Magalhães, A.; *J. Braz. Chem. Soc.* **2011**, *22*, 961.
2. Wang, Y. J.; Price, A. D.; Caruso, F.; *J. Mater. Chem*. **2009**, *19*, 6451.
3. Frederice, R.; Ferreira, A. P. G.; Gehlen, M. H.; *J. Braz. Chem. Soc*. **2010**, *2*, 1213.
4. Schuetz, W.; Caruso, F.; *Chem. Mater.* **2002**, *14*, 4509.
5. Santra, S.; Zhang, P.; Wang, K. M.; Tapee, R.; Tan, W. H.; *Anal. Chem.* **2001**, *73*, 4988.
6. Santra, S.; Wang, K. M.; Tapee, R.; Tan, W. H.; *J. Biomed. Opt.* **2001**, *6*, 160.
7. Li, H.; Fu, Y. Q.; Zhang, L. B.; Liu, X. M.; Qu, Y.; Xu, S. T.; Lü, C. L.; *Microporous Mesoporous Mater*. **2012**, *151*, 293.
8. Yan, F.; Wang, Y.; He, S. Z.; Ku, S. T.; Gu, W.; Ye, L.; *J. Mater. Sci.: Mater. Med.* **2013**, *24*, 2371.
9. Vankayala, R.; Gollavelli, G.; *J. Mater. Sci.: Mater. Med.* **2013**, *24*, 1993.
10. Mumin, A. M.; Barrett, J. W.; Dekaban, G.A.; Zhang, J.; *J. Colloid. Interface Sci.* **2011**, *353*, 156.
11. Han, B. H.; Manners, I.;Winnik, M. A.; *Chem. Mater.* **2005**, *17*, 3160.
12. Lu, D. L.; Lei, J. Y.; Tian, Z. D.; Wang, L. Z.; Zhang, J. L.; *Dyes Pigm.* **2012**, *94*, 239.
13. Latterini, L.; Amelia, M.; *Langmuir* **2009**, *25*, 4767.
14. Wang, L. L.; Li, B.; Zhang, L. M.; Zhang, L. G.; Zhao, H. F.; *Sens. Actuators, B* **2012**, *171*, 946.
15. Wolfbeis, O. S.; *Anal. Chem.* **2006**, *78*, 3859.
16. Kros, A.; Gerritsen, M.; Sprakel, V.; Sommerdijk, N.; Jansen, J.; Nolte, R.; *Sens. Actuators, B* **2001**, *81*, 68.
17. Couto, C.; Araujo, A.; *Talanta* **2002**, *56*, 997.
18. Yang, H. P.; Zhu, Y. F.; *Talanta* **2006**, *68*, 569.
19. Campbell, D. W.; Muller, C.; Reardon, K. F.; *Biotechnol. Lett*. **2006**, *28*, 883.
20. Endo, H.; Yonemori, Y.; Musiya, K.; Maita, M.; Shibuya, T.; Ren, H.; Hayashi, T.; Mitsubayashi, K.; *Anal. Chim. Acta* **2006**, *573*, 117.
21. Reardon, K. F.; Campbell, D. W.; Muller, C.; *Eng. Life Sci.* **2009**, *9*, 291.
22. Wang, Y. H.; Fan, W.; Nugen, S. R.; *Mater. Lett*. **2013**, *92*, 17.
23. Wang, W.; Yan, X. L.; Zhan, L.; Leng, F.; Yang, X. X.; Huang, C. Z.; *Chin. Sci. Bull.* **2014**, *59*, 147.
24. Zhou, L. M.; Huang, J. S.; Yang, L.; Li, L. B.; You, T. Y.; *Anal. Chim. Acta* **2014**, *824*, 57.
25. Liu, Q.; Deshong, P.; Zachariah, M. R.; *J. Nanopart. Res.* **2012**, *14*, 923.
26. Li, T.; Yao, Z. H.; Ding, L.; *Sens. Actuators, B* **2004**, *101*, 155.
27. Huang, J.; Wang, H.; Li, D. P.; Zhao, W. Q.; Ding, L. Y.; Han, Y.; *Mater. Sci. Eng., C* **2011**, *31*, 1374.
28. Rossi, L. M.; Shi, L. F.; Quina, F. H.; Rosenzweig, Z.; *Langmuir* **2005**, *21*, 4277.
29. Bradford, M. M.; *Anal. Biochem.* **1976**, *72*, 248.
30. Huo, X. H.; Liu B. I.; Deng, X. B.; Zhang, B. T.; Chen, H. I.; Luo, R.; *Anal. Biochem.* **2007**, *368*, 100.
31. Posthumus, W.; Magusin, P. C. M. M.; Brokken-Zijp, J. C. M.; Tinnemans, A. H. A.; van der Linde, R.; *J. Colloid Interface Sci*. **2004**, *269*, 109.
32. Arkles, B.; Steinmetz, J. R.; Zazyczny, J.; Mehta, P.; *J. Adhes. Sci. Technol.* **1992**, *6*, 193.
33. Pham, K. N.; Fullston, D.; Sagoe-Crentsil, K.; *Aust. J. Chem.* **2007**, *60*, 662.
34. Ahmad, A.; Akhtar, M. S.; Bhakuni, V.; *Biochemistry* **2001**, *40*, 1945.
35. Lo, Y. L.; Chu, C. S.; Yur, J. P.; Chang, Y. C.; *Sens. Actuators, B* **2008**, *131*, 479.

Submitted: May 5, 2015
Published online: July 3, 2015